Indiana State University

Sycamore Scholars

2012

Remote Sensing of Tanzanian Volcano Oldoinyo Lengai: Verifying Detection Methods of Flow Activity

Scott Richard Frystak
Indiana State University

Follow this and additional works at: https://scholars.indianastate.edu/etds

Remote Sensing of Tanzanian Volcano Oldoinyo Lengai:

Verifying Detection Methods of Flow Activity

––––––––––––––––––––––

A Thesis

Presented to

The College of Graduate and Professional Studies

Department of Earth & Environmental Systems

Indiana State University

Terre Haute, Indiana

––––––––––––––––––––––

In Partial Fulfillment

of the Requirements for the Degree

Earth & Quaternary Sciences

––––––––––––––––––––––

by

Scott Richard Frystak

Planned Graduation Date: December 2012

Keywords: Oldoinyo Lengai, Remote Sensing, Volcano, Flow Activity

COMMITTEE MEMBERS

Committee Chair: Stephen Aldrich, Ph.D.

    Assistant Professor of Geography

    Indiana State University

Committee Member: Sandra Brake, Ph.D.

    Associate Professor of Geology

    Indiana State University

Committee Member: Qihao Weng, Ph.D.

    Professor of Geography

    Indiana State University

ABSTRACT

Every day volcanoes erupt with varying magnitudes across the globe, and remote sensing used to keep track of volcanic activity would be a useful application. One promising use of remote sensing to understand volcanoes at a distance is to distinguish gaseous or lava flow activity. Current methods for differentiating volcanic activity with remote sensing have only been applied at Mt. Etna, and research is still needed to verify that the detection of gaseous or lava flow activity is possible at volcanoes with different compositions. The subject of this study, the Oldoinyo Lengai volcano, is a natrocarbonatite stratovolcano with drastically different chemical composition from Mt. Etna. These composition differences allow for the verification of gaseous or lava flow activity remotely over time. Furthermore, looking closely at how volcano composition affects detection will allow us to understand the variables required to detect gaseous or lava flow activity. The results of the research are inconclusive, but provide useful information for this application of remote sensing. For Oldoinyo Lengai, the Landsat TM data were unable to resolve lava flows or degassing activity, due to a combination of the volcano's small size, the lack of lava flows, and/or pixel saturation. Superior sensors such as hyperspectral sensors are needed to adequately perform the analysis, and would likely result in the capability to differentiate volcanic activity. Further applicability of the study is prudent due to the varying nature of volcanoes and sensors. Gathering additional detailed information should be at the forefront of volcanic monitoring research.

ACKNOWLEDGMENTS

I wanted to acknowledge Indiana State University for providing an environment useful and enjoyable for working on my Masters Degree. I also thank the Indiana State University School for Graduate and Professional Studies for supporting me with a tuition waver and stipend to help me attend this institution. I wanted to thank my committee members for helping me complete my thesis. I also wanted to thank all the other graduate and undergraduate students that made my graduate school experience an enjoyable time. Finally, I wanted to thank my mother Jeannine Jonas, and my father Paul Frystak in supporting me throughout the process of my graduate studies.

TABLE OF CONTENTS

LIST OF TABLES

LIST OF FIGURES

CHAPTER 1

INTRODUCTION

Volcanic eruptions occur daily across the globe and much of this activity remains

unmonitored beyond very simple visual or seismic data, collected in a limited fashion. Typically,

only those volcanoes that implicitly or actually threaten large populations or significant

infrastructure are monitored regularly. This leaves an extremely large gap in the awareness of

potentially important volcanic activity, particularly in remote locations and at volcanoes

presumed extinct. One method to address this data shortcoming would be through the

application of remote sensing techniques to regularly monitor volcanoes without draining

significant resources with physical visits.

Ever since the launch of Landsat Thematic Mapper (TM), the ability to look at volcanoes

from afar has increased substantially, allowing one to discern volcanic features, not just in the

visible range of light, but also in the thermal portions of the electromagnetic spectrum. Over

time, it has become possible to view volcanoes with superior spectral and spatial resolutions on

shorter temporal scales. As the applications of multispectral remote sensing have expanded

research has approached the problem of volcano monitoring using remote sensing. One of these

approaches is the Dual Band Equation (DBE), developed by Dozier (1981), which estimates two

separate temperature components (cold temperature and hot temperature) within one pixel

(Dozier, 1981). A few years later, Rothery and colleagues used a similar equation with Landsat

TM data (Rothery et al. 1988). Lombardo et al. (2004; 2006) extended these initial works by relating variables used in the DBE for basaltic lava flows and degassing activity on Mt. Etna in Italy, further characterizing thermal anomalies.

Given that Mt. Etna is a basaltic stratovolcano with a globally common composition (GVP, 2011a), the conclusions of Lombardo et al. (2004) are useful, but their method has not been shown to function for other volcanic compositions. Since many volcanic compositions exist across Earth, applying the methods Lombardo et al. (2004) used at Mt. Etna to volcanoes with different compositions will address a gap in the literature; the DBE may provide similar information for non-basaltic volcanoes in other locales. In the research described here, the DBE will be applied to a natrocarbonatite volcano in Tanzania named Oldoinyo Lengai (OL), which is compositionally different than Mt. Etna. The overarching research objective is to see if lava and gaseous activity can be detected at OL using methods similar to those employed by Lombardo et al. (2004), despite its compositional differences from Mt. Etna. In pursuit of this goal, the relationship between sub-pixel variables will be examined, which could indicate the type of volcanic activity at OL. To further validate the findings, the goal is to investigate these sub-pixel relationships across many images. If the relationships were to be seen at OL using the methods Lombardo et al. (2004) employed at Mt. Etna, it would help bolster the case for applying DBE methods to monitor volcanoes of varying composition elsewhere. If these specific relationships between the sub-pixel variables were not found at OL, then the next logical objective would to find what relationship does exists between the sub-pixel variables and volcanic activity at OL.

A sub-objective of this project was to see if the relationship between key variables derived from OL using the DBE is similar to the relationship observed at Mt. Etna by Lombardo et al. (2006). Potential problems were possible due to the spatial resolution of Landsat TM data;

since Landsat TM data has moderate spatial resolution it may be that the relationships between key variables at OL are unresolvable. Another sub-objective is of the study is to examine relationships between key variables resulting from the DBE as lava flows progress and move down slope. What will the relationship look like at the summit, along the flow, or at the distal portions of the flow? This is important because flow activity changes as the flow progresses away from the vent, cooling on the surface and becoming thermally indistinguishable from background surfaces. The lava flows become indistinguishable when the top of the flow cools with a solid top. The temperature above the solidified flow will be extremely close to the ambient temperature around the cooled flow. This is important to note because the DBE methods will only yield results if an image of a lava flow before it cools is available.

Once the relationship between sub-pixel variables is found, the relationships similarity to the Lombardo et al. (2006) study needs to be assessed. One important question is if changes in the sub-pixel relationships are seen due to compositional differences between Mt Etna and OL. This can be evaluated by using Landsat TM data to replicate the DBE analysis at Mt. Etna. When sub-pixel relationships are different when compositional differences between the volcanoes are controlled, then it is extremely important to understand what causes that change. One potential cause may be the difference in spatial resolution between the imagery. However, the overall relationship between sub-pixel variables should be similar to the Lombardo et al. (2006) study.

CHAPTER 2

LITERATURE REVIEW

Satellites and Sensors

Landsat 1, was launched in 1972 and was the first in a series of sensors that are used to

look at surface objects. Landsat Multispectral Scanner (MSS), Landsat Thematic Mapper (TM),

and Enhanced Thematic Mapper Plus (ETM+) sensors are used to observe different surface

objects. The Thematic Mapper, which is used in this study, was installed on Landsat 4 and 5,

and produces data in 7 bands, or divisions of the electromagnetic spectrum. Bands 1 through 5

and 7 have a spatial resolution of 30 meters and use pixels (a pixel is shorthand for "picture

element") to represent this data. Bands 1, 2, and 3 are within the visible spectrum ranging from

0.45 to 0.52, 0.52 to 0.60, and 0.63 to 0.69 micrometers respectively, corresponding to blue,

green, and red light wavelengths (again, respectively). Band 4 ranges from 0.76 to 0.90

micrometers: just past the visible spectrum in the so-called "near infrared" range. Bands 5 and 7

are within the shortwave-infrared ranging from 1.55 to 1.75 and 2.08 to 2.35 micrometers

respectively, and are used to analyze thermal data in this study. Band 6 has a spatial resolution

of 120 meters in thermal infrared light with a wavelength range from 10.42 to 12.42

micrometers. These were the first set of sensors used to adequately view volcanoes (Flynn et al.

2001) beyond the visible spectrum. Landsat TM has detailed enough spectral resolution, or the

division of the electromagnetic (EM) spectrum, to resolve volcanic temperatures. Because these

sensors have become so advanced, we can now use them to look at surface object with more detail: and in this case the volcano Oldoinyo Lengai.

The Landsat 7 Enhanced Thematic Mapper Plus (ETM+) is also used to monitor volcanoes. It has a 15 meter panchromatic band, band 8, and can be used to look at smaller features that would have been unobservable with coarser resolutions. The Landsat ETM+ thermal band 6 has a resolution of 60 meters with high and low gain settings opposed to the 120 meter on the Thematic Mapper sensor with fixed gain. The ETM+ low gain settings increase from roughly 13 $W/m^2/sr/\mu m$ to roughly 17 $W/m^2/sr/\mu m$, and are used to view higher temperature features due to less pixel saturation afforded by the gain settings. Band 7 has a slightly narrower wavelength range by $0.01\mu m$, allowing for more precise measurements (Flynn et al. 2001). Landsat 7 also has the standard visible and shortwave infrared bands on Bands 1 through 5 and 7 (with similar radiometric characteristics to the TM sensor). Future satellites such as the Landsat Data Continuity Mission will contain similar sensors to the ETM+ that can be used to observe volcanoes. With new sensors, we can perform superior analyses to better understand volcanoes.

Lombardo et al. Studies

Valero Lombardo and his associates have worked on identifying thermal anomalies in a number of published articles, all of which are important in the application described in this thesis. Two studies are particularly important; the 2006 study in Bulletin of Volcanology called "Characterization of volcanic thermal anomalies by means of sub-pixel temperature distribution analysis," and the 2009 article in Journal of Geophysical Research titled "Spatial variations in lava flow field thermal structure and effusion rate derived from very high spatial resolution hyperspectral (MIVIS) data."

Lombardo et al. 2006

This study uses a hyperspectral airborne sensor called the Digital Airborne Imaging

Spectrometer (DAIS) 7915 spectrometer to take images of Mt. Etna, a volcano located in Sicily,

Italy. These DAIS data were selected for its high spatial resolution of 2 to 20 meters and its 15

bit dynamic (spectral) range. These two qualities are important because they reduce the number

of saturated pixels (pixel saturation occurs if the light measured in a specific band becomes

intense enough to produce a maximum response, essentially producing unusable data, similar to

a "blown out" photograph). The DAIS data also increases the number of usable pixels relative to

AVHRR and Landsat TM data due to its higher spatial resolution (Lombardo et al., 2006).

To process the DAIS data, two Short Wave Infrared (SWIR) bands were used calculate

T_c and f_h with two equations:

(01) $\qquad R\alpha = f_h(R_h\alpha) + (1 - f_h)R_c\alpha$

(02) $\qquad R\beta = f_h(R_h\beta) + (1 - f_h)R_c\beta$

These two equations are a summarized version of the dual band system equation from Rothery et

al. (1988) adapted for DAIS data. f_h is the fractional area of the hot portion of the pixel, $R\alpha$ and

$R\beta$ are the total radiance in each respective band. $R_c\alpha$ and $R_c\beta$ are the radiance values calculated

for the cold portion of the pixel in each band and $R_h\alpha$ and $R_h\beta$ are the radiance values for the

hot portion of the pixel for each band (Lombardo et al., 2006).

Additionally, after the equations in this article were used, other variables T_c (temperature

of the cold portion of the pixel) and f_h were calculated and used to create scatter plots. These

two variables were shown to have specific trends for lava flows or degassing activity. For the 16

July 1996 lava flow, plotted DAIS data exhibit a trend of $T_c = 61 \ln(f_h) + 652$ with an R^2 of

0.67. Data for the 18 July 1996 lava flow plot exhibit a trend of $T_c = 59 \ln(f_h) + 667$ with an R^2

of 0.76. Both of these polynomial trends represent lava flow activity. Possible values for lava

flow activity can be seen in Figure 1. A general trend is established in Figure 2 with T_c values

ranging from roughly 100 to 400 degrees Celsius and f_h values range from 0 to 0.008.

Figure 1. A Scatterplot Showing Possible Values for Lava Flow Activity
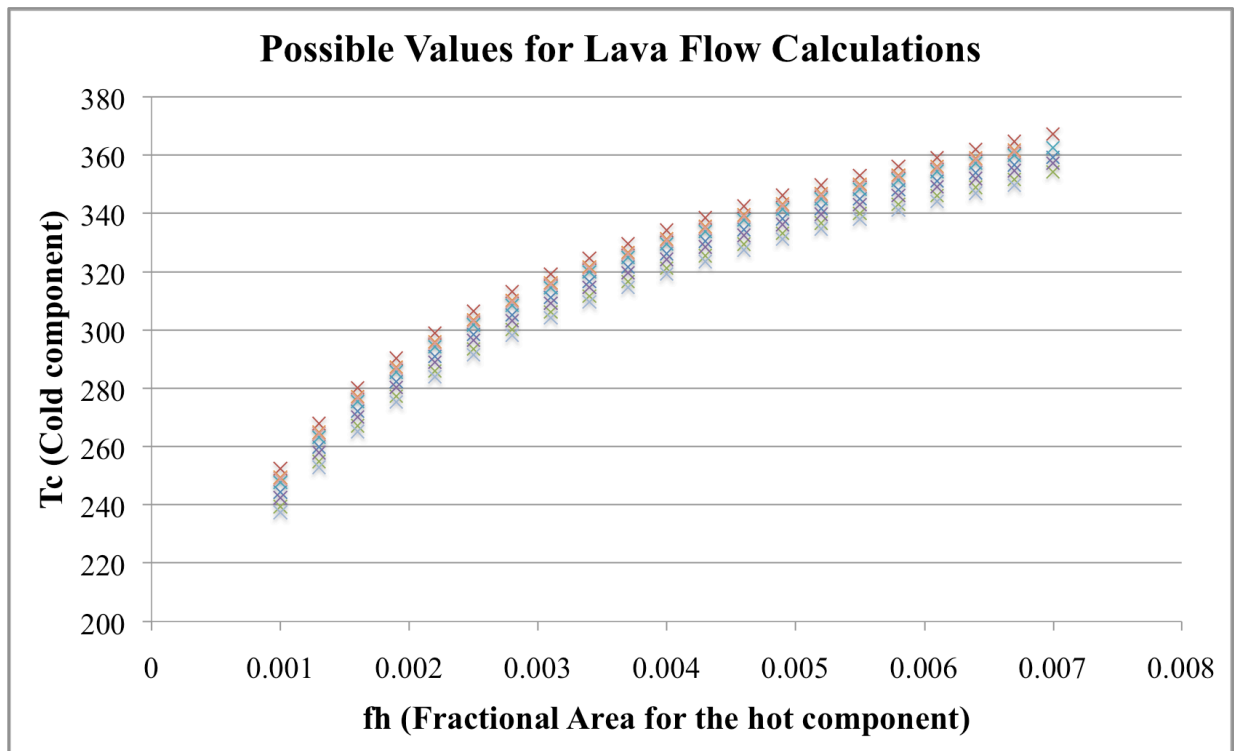
Figure 2. Shows the General Trend of Possible Values for Areas of Lava Flow Activity
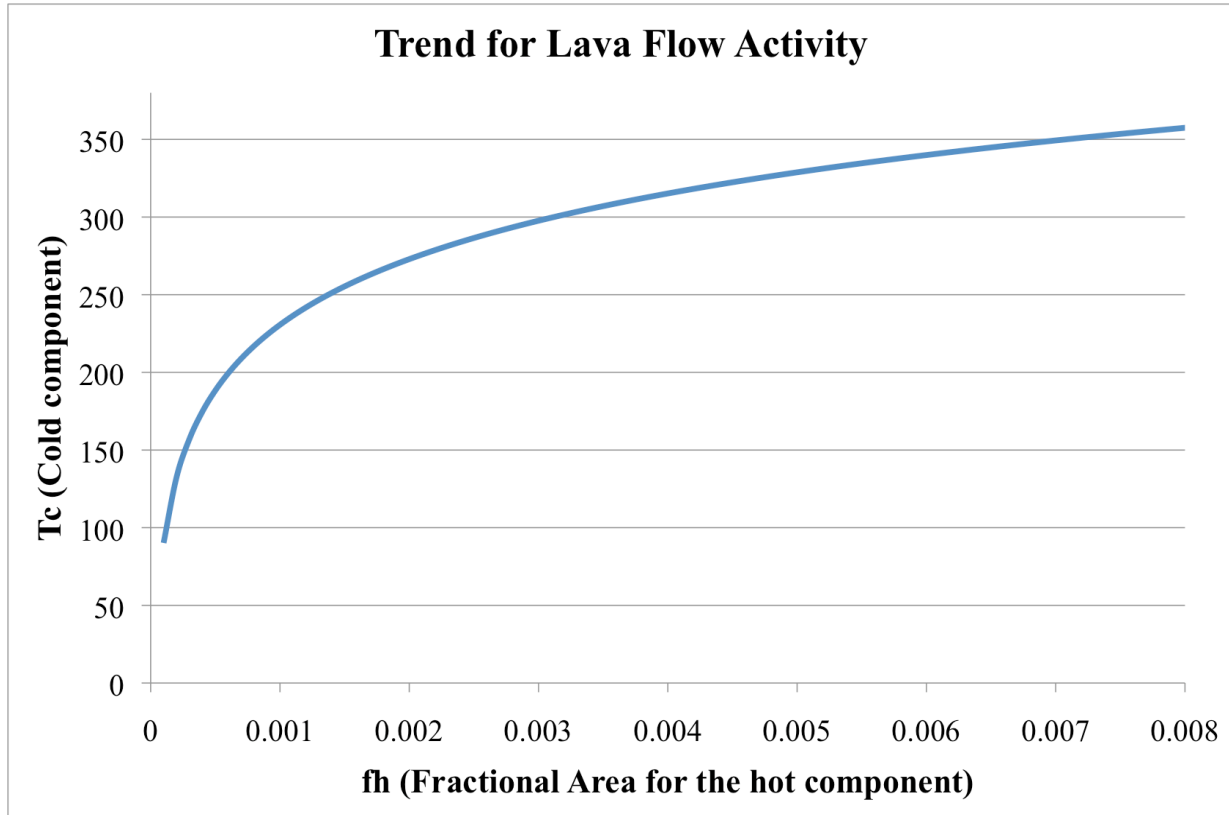
Another trend is seen with degassing activity at a crater hot spot; with these crater data points, as

T_c rises f_h remains relatively constant, creating a distinguishable trend for degassing activity.

Possible values for degassing activity can be seen in Figure 3, with T_c values range from around

150 to 400 degrees Celsius, and f_h values generally range from 0 to 0.002. The established trend

for degassing activity is seen in Figure 4, with T_h values max out just over 400 degrees Celsius,

and f_h values do not exceed 0.002 unless near the higher temperatures.

Figure 3. A Scatterplot of Possible Values that may Occur From an Image Processed with

Volcanic Degassing Activity
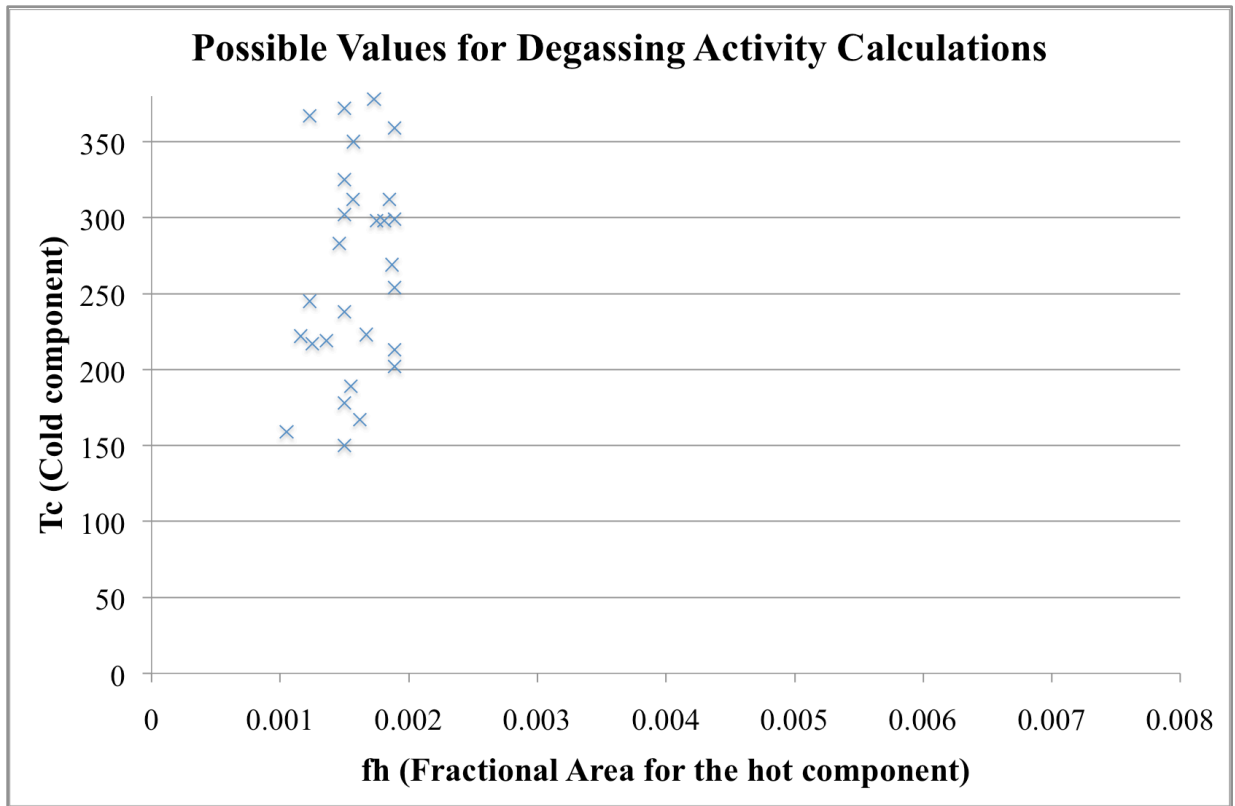
Figure 4. This Trend Shows the Upper Limits of Possible Values Occurring from an Image of

Volcanic Degassing Activity

Upper Limit for Values of Degassing Activity
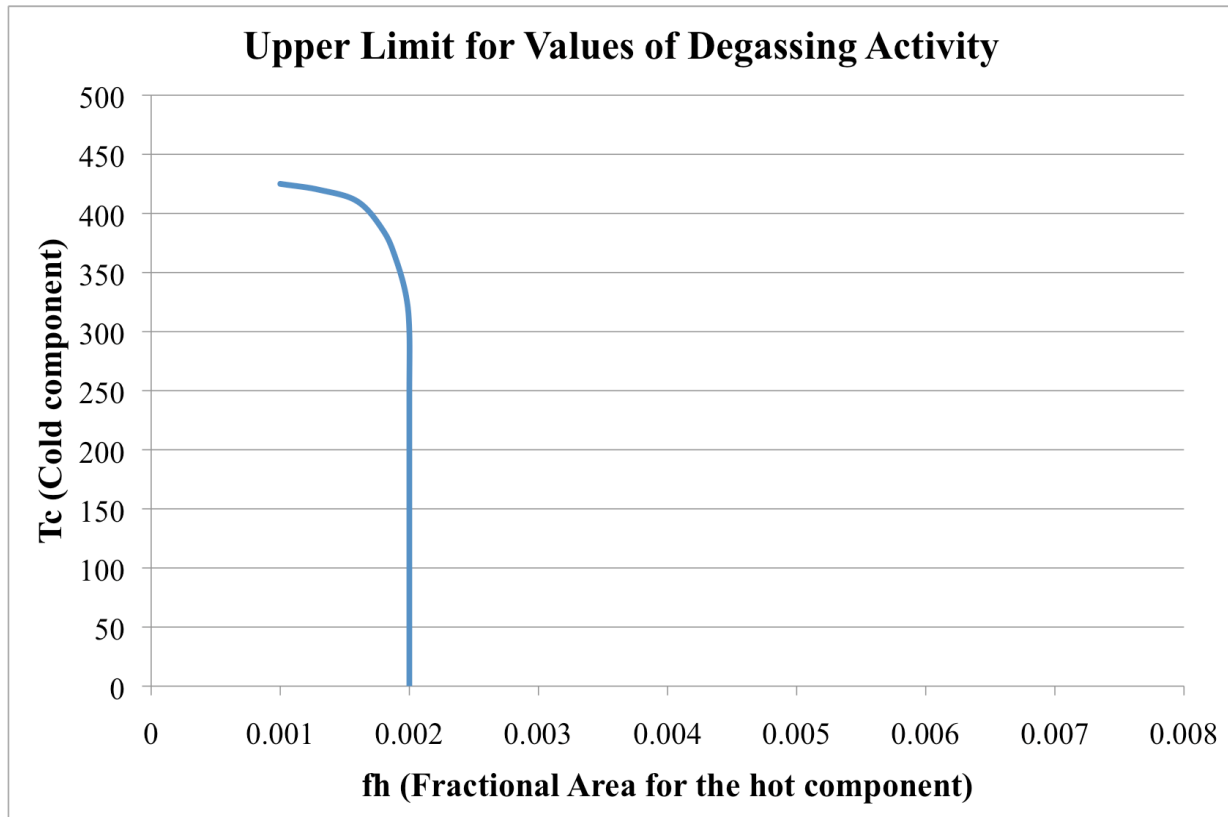
These three trends show that using equations 1 and 2, and plotting T_c with f_h, scatter plot trends

can be created allowing lava flow and degassing activity to be distinguished. The intended goal

of this study is to show that different types of flow activity either lava flows or degassing activity

can distinguished by creating scatter plots of T_c vs. f_h, replicating some aspects of the approach

described by Lombardo et al. (2006).

Lombardo et al. 2009

In the Lombardo et al. (2009) study, the objective was similar to the 2006 study.

Hyperspectral data from the airborne sensor known as the Multispectral infrared and visible

imaging spectrometer (MIVIS) was used to image an eruption at Mt. Etna on July 29, 2001. An

adaption of the methods described by Rothery et al. (1988) was used to create an equation which

calculated T_c, and T_h, the hot and cold temperatures of the feature, and the fractional areas the

hot and cold features occupy, f_c, and f_h:

(03) $L(T_x\lambda_x) = \varepsilon_x\tau_x [f_cL(T_c\lambda_x) + (1-f_c)L(T_h\lambda_x)]$

Equation 03 employs two shortwave infrared bands to calculate the sub-pixel variables.

Lombardo et al. (2009) modified equation 3 so that sub-pixel variables were calculated using two

short wave infrared bands and one thermal infrared band. Lombardo et al. (2009) applies this

modification to different bands with the following equation:

(04) $R_x = \varepsilon_x [f_h (Rh_x) + (1-f_h)Rc_x]$

R_x is the radiance in band x, Rh_x and Rc_x are the hot and cold radiances for the hot and cold

portions of the pixel respectively. By using three bands, none of the sub-pixel variables need to

be assumed, thus creating a stronger analysis (Lombardo et al., 2009).

Thermal anomalies on the July 29, 2001 study revel that there are a total of seven active

lava flow fields on Mt. Etna during the study period. T_h solutions range from 350 to 1,077

degrees Celsius and are comparable to ground measurements. T_c solutions for thermal

anomalies range from 190 to 440 degrees Celsius. Three trends between T_c and f_h are observed;

the first is a nearly vertical trend of values along the T_c axis, the second is shown when T_c

increases f_h decreases, the final trend shows a unimodal distribution of T_c at 280 degrees

Celsius. Considering lava flows, values for T_c and f_h tend to occur towards the core of the

thermal anomalies. In this study, using hyperspectral data allowed for more values to be

calculated, due to the high spatial resolution capturing more pixels, while maintaining higher

accuracy, due to the high dynamic range and spectral resolution of such sensors, which

ameliorates problems with pixel saturation.

In both of these studies, scatterplots of f_h and T_c allow for distinction of lava styles. Techniques such as these can be used on volcanoes where field measurements are difficult (Lombardo et al., 2009), saving time and financial resources and allowing for the development of truly global eruption monitoring systems.

CHAPTER 3

STUDY AREA

Oldoinyo Lengai

Oldoinyo Lengai (OL) is a small stratovolcano around 3,000 meters in diameter, located in the Gregory Rift Valley of Tanzania, at 2.764 degrees south, by 35.914 degrees east (GVP, 2011b). The location of Oldoinyo Lengai can also be seen in Figure 5. The location map shows the location of OL relative to the entirety of Africa, and shows its regional location near the Kenya/Tanzania boarder. This volcano was first recognized in 1960 as productive of high alkali carbonate lavas (Dawson, 1962), later termed natrocarbonatite (Du Bois, 1963). Researchers determined that OL was a natrocarbonatite volcano in 1960 (Dawson, 1962). Since that point there has been considerable interest in the volcano given its unusual composition. Many expeditions to the summit of OL have been undertaken, even recently. Although OL is not actively monitored, the literature provides sufficient information on the general periods of eruptions, quiescence, and its dynamic chemical history (Dawson et al., 1990). All important eruption periods with information about each are listed in Table 1, with the earliest observations start in the late 1800's to modern day (Keller et al. 2010).

Figure 5. A Location Map of Oldoinyo Lengai
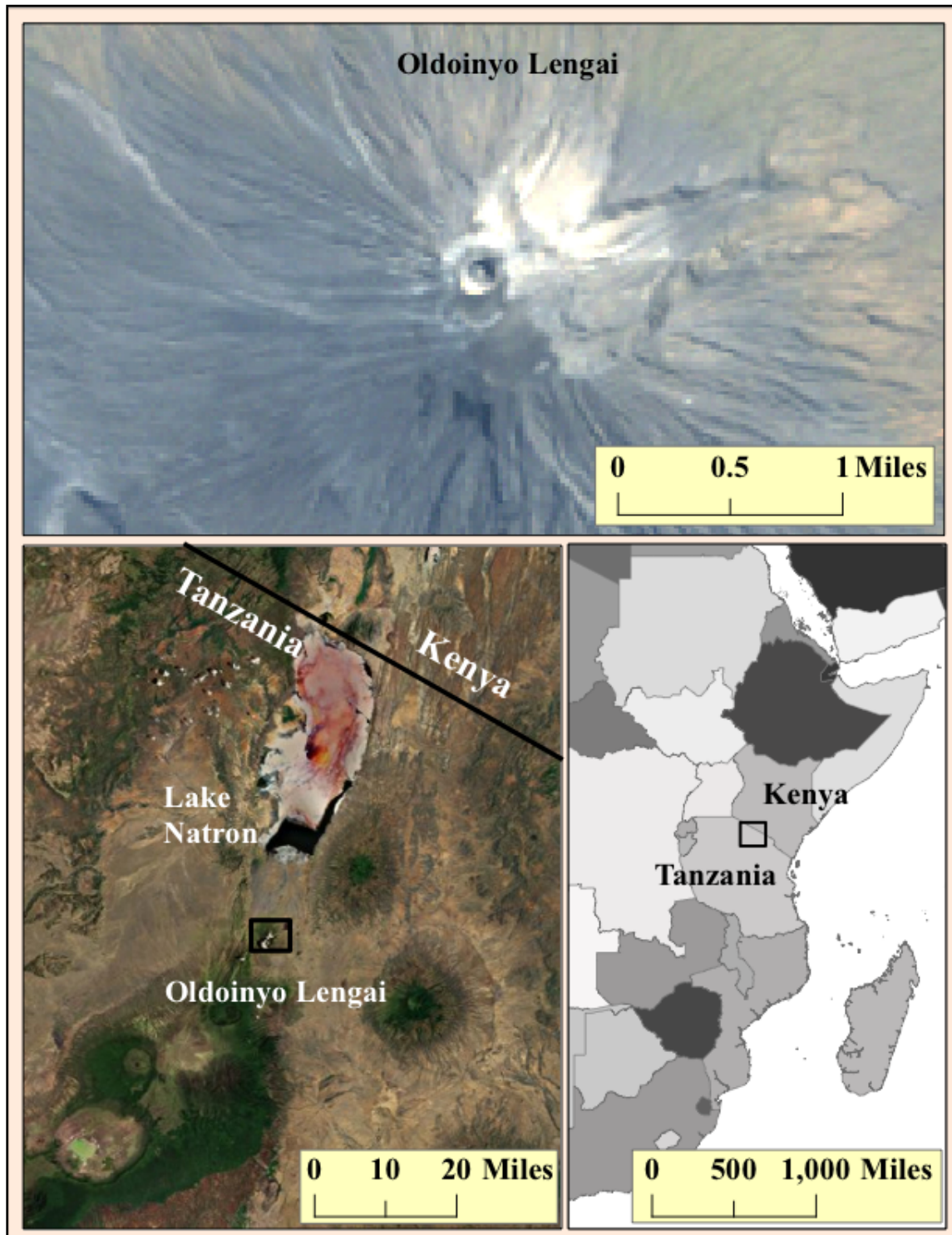
Table 1. All Important Eruptions and Periods of Quiescence at Oldoinyo Lengai

Activity Date	Volcanic information.
1880	First reports by explorers of snow and smoke on the summit with reported volcanic activity from the local population.
1904	First climb by F. Jaeger.
1904-1915	Sodaschlammströme inferred natrocarbonatite effusive activity. Changes in hornito in photos taken in 1904 and 1915.
1917	Major eruption with ash, nephelinite lavas and agglomerates. The geologic record indicates nephelinite lavas and agglomerates above the carbonatite platform forming the western and eastern rim.
1921, 1926	Minor eruptions reported.
1940-41	Explosive eruption with soda rich ashes. Geologic record of serge series between 1917 and 1966/67 with pyroclasts at the summit. Ash, spherical lapilli, and a bomb field. Also contained mixed ashes of silicate and carbonatite.
1954-55	Minor eruptions reported.
1960	Effusive activity. First acknowledgment of natrocarbonatites.
1966-1967	Explosive eruptions with mixed ashes. Geologic record indicates grey series of ashes with spherical combeite-wollastonite-nephelinite lapilli on all slopes.
1983	Minor explosive eruption reported, most likely natrocarbonatite.
1988-2007	Consistent documentation of effusive natrocarbonatite activity.
2007-2008	September 4th 2007 explosive paroxysm with explosive eruption plumes higher than 10km. Geologic record shows ashes, lapilli and scoriae of carbonated combeite-wollastonite-melilite nephelinite.

Mineralogy and Chemistry

Over the past few decades researchers have collected mineralogical samples of OL's

lava. Minerals form at OL from lava degassing while cooling, atmospheric alteration and

hydration by fresh water, or from reaction with fumarole gases, forming in different abundances

depending on the originating environment. These minerals include: nahcolite, trona,

thermonatrite, halite, sylvite, aphthitalite, kalicinite, villiaumite, pirssonite, gaylussite, shortite,

kogarkoite, calcite, sulphur, gypsum, anhydrite, monohydrocalcite, flourite, barite and celestine,

and are listed in Table 2 with their method of formation. In Table 2 major minerals are signified

by +++, minor minerals are signified by ++, and accessory minerals are signified by + (Zaitsev and Keller, 2006).

Table 2. "Subsolidus Minerals in Oldoinyo Lengai Natrocarbonatites." (Zaitsev and Keller, 2006)

Minerals	Minerals formed due to…		
	Lava degassing during cooling	Atmospheric alteration and hydration by meteoric waters	Reaction with fumarole gases
Nahcolite	+++	+++	
Trona	+++	+++	
Thermonatrite	+++	+++	
Halite	+++		
Sylvite	+++		
Aphthitalite	++	+	
Kalicinite	+		
Villiaumite	+		
Pirssonite		+++	
Gaylussite		+++	
Shortite		+++	
Kogarkoite		+	
Calcite		+++	+++
Sulphur			+++
Gypsum			+++
Anhydrite			++
Monohydrocalcite			++
Flourite		+	++
Barite			++
Celestine			+

In addition to mineralogical information, lava chemistry analyses have also been conducted at OL. The lavas at OL weather very quickly relative to other composition lavas, based on the three external factors of water, temperature, and time. The most abundant sources of mineral altering water are from atmospheric water, fog, and rain. The temperature of the atmosphere will affect how soluble each mineral becomes. Extensive changes in the mineralogy on the lava surface will typically become evident after several time intervals. Samples of the

lava from 2 to 24 hours after solidification show alteration minerals: nahcolite, trona, sylvite and halite with the accessory minerals kalicinite and villiaumite (Zaitsev and Keller, 2006).

Almost immediately after extrusion, the natrocarbonatite lavas begin to alter. The stages of natrocarbonatite alteration are not fully understood, but within a few days the black natrocarbonatite lavas alter from a white to grey powdery unconsolidated soil like texture. Within the following year the flows have been seen to fully alter containing high amounts of CaO, F, H_2O while reducing in amounts of Na_2O, K_2O and traces of other elements, as seen in Table 3 (Zaitsev and Keller, 2006). The samples in Table 3 were analyzed to view how the chemical makeup of natrocarbonatite lava changes due to weathering. It is possible to see chemically how the lavas change through weathering by looking at the drastic changes between sample types in the following chemicals CaO, Na_2O K_2O and others. In Table 4 fresh natrocarbonatites include samples 1 and 2, partially weathered are contained by samples 3 through 7, and weathered samples include 8, 9 and 10: adaption from Zaitsev and Keller (2006).

Table 3. The Following Natrocarbonatite Lava Samples were Taken in 2000 at OL

	Fresh natrocarbonatite		Partially weathered natrocarbonatite					Weathered natrocarbonatite		
Sample	1.00	2.00	3.00	4.00	5.00	6.00	7.00	8.00	9.00	10.00
SiO_2	0.34	0.26	1.59	0.17	0.10	0.64	0.11	0.69	0.40	1.00
TiO_2	0.01	0.01	0.06	0.01	0.01	0.03	0.01	0.04	0.03	0.00
Al_2O_3	0.04	0.05	0.25	0.01	0.01	0.03	<0.01	0.05	0.02	0.00
Fe_2O_3	0.65	0.58	1.84	0.47	0.16	2.38	0.20	1.88	1.20	0.00
MnO	0.46	0.44	0.88	0.79	0.54	0.63	0.56	1.25	1.11	0.00
MgO	0.42	0.44	0.55	0.66	0.56	<.10	0.59	0.83	0.52	1.00
CaO	16.40	15.83	27.57	26.50	27.79	24.99	27.69	46.07	45.91	46.00
SrO	1.33	1.39	1.53	1.60	1.91	1.73	1.91	3.39	3.54	3.00
BaO	0.96	1.17	1.04	1.05	1.62	1.20	1.61	2.45	2.99	4.00
Na_2O	33.68	33.08	23.21	24.13	21.67	22.69	21.89	1.73	2.91	2.00

Table 3, continued.

Continuation of Table 3.

	Fresh natrocarbonatite		Partially weathered natrocarbonatite				Weathered natrocarbonatite			
K_2O	7.04	7.43	0.78	2.29	0.32	0.34	0.75	0.19	0.20	0.00
P_2O_5	1.13	0.90	1.21	1.09	0.77	1.06	0.74	2.68	1.51	0.00
CO_2	32.49	32.80	33.55	34.30	31.40	31.94	30.65	33.18	33.80	29.00
Cl	2.64	2.87	0.04	0.08	<0.01	0.02	0.01	<0.01	0.08	0.00
SO_3	2.32	2.25	0.28	0.40	0.25	0.02	0.30	0.24	0.05	0.00
F	1.20	1.10	1.63	1.32	2.13	1.40	2.88	3.64	6.62	9.00
H_2O	0.14	0.17	5.37	7.29	10.00	11.70	12.00	0.84	0.86	1.00
-O=F, Cl	1.10	1.11	0.70	0.57	0.90	0.59	1.22	1.53	2.81	3.00
Total	100.15	99.66	100.68	101.59	98.34	100.21	100.68	97.62	98.94	98.00

There are many types of volcanoes and volcanic compositions. One main objective of this study was to see if the differences in volcanic composition will affect the analysis of the remote sensing images. It is likely that there are chemical differences between the lavas at OL and Mt. Etna. Understanding any chemical differences, and how satellites view their representation in the images is very important. These differences could be observable through changes in temperature or difference in the surface area of each lava flow.

Mount Etna Lavas

One of the overarching ideas of this study was that images of OL are likely show a different relationship between sub-pixel variables than Mt. Etna, most likely from the differences in lava composition. A chief difference between the two volcanoes is that OL has predominantly natrocarbonatite lavas, while Mt. Etna has typically exhibited trachybasalts from 1995 to 1999. By comparing Tables 3 and 4, differences in lava chemistry between OL and Mt. Etna become apparent. Some major elemental differences between OL and Mt. Etna are: SiO_2, Al_2O_3, Na_2O, and Cl, among many others (Corsaro and Pompilio, 2004). Table 4 shows activity at the

northeast crater from December 1995 to March 1998. The July 24th 1996 sample taken at Mt.

Etna is temporally close to the samples that Lombardo et al. (2006) took on July 18th 1996.

Sample types are indicated as either F (fire fountain lapilli and bombs) or L (quenched lava).

The data was adapted from Corsaro and Pompilio (2004).

Table 4. The Following Table Shows Chemical Analyses of Lava Taken at Mt. Etna

Date	23 Dec '95	10 Feb '96	24 Jul '96	27 Mar '98
Sample type	F	F	L	F
No. of Analyses	3.00	3.00	24.00	9.00
SiO_2	48.87	48.92	48.85	49.57
TiO_2	2.03	2.07	2.06	1.94
Al_2O_3	16.27	16.41	15.83	16.87
FeO_{tot}	10.23	10.34	10.55	10.41
MnO	0.00	0.00	0.34	
MgO	4.11	3.80	3.08	3.65
CaO	8.29	8.20	7.28	7.28
Na_2O	4.69	4.66	5.01	5.61
K_2O	2.99	2.98	3.56	3.18
P_2O_5	0.70	1.00	1.09	0.92
Cl	0.19	0.16	0.20	0.18
Total	98.37	98.54	97.85	100.11
CaO/Al_2O_3	0.51	0.50	0.46	0.46
$FeOtot/MgO$	2.49	2.72	3.42	2.85
T (°C)	1114.00	1104.00	1083.00	1098.00

At Mt. Etna, the lavas are strongly porphyritic while containing commonly erupted

minerals such as plagioclase, clinopyroxene, olivine, with Ti-magnetite both as phenocrysts and

groundmass (Corsaro and Pompilio, 2004). The mineralogy of the lava directly affects the

viscosity, and temperature of the flow, with higher temperature and lower viscous flows having a

greater extent on the landscape given the proper topography. Lavas at Mt. Etna have high

volumes, and topography favors down slope flows, which is seen by aerial or satellite imagery. The lavas at OL have low viscosity, yet topography favors pooling given the crater is where most lava extrusion occurs. In a few cases, enough volume was extruded to flow over the crater rim and down the slopes (Vaughan et al., 2008).

CHAPTER 4

DATA AND METHODS

Dual Band Technique

Using satellites it is possible to view planetary surfaces as pixels that contain different types of information, such as digital numbers. These digital numbers on Landsat TM range from values 0 to 255 and represent a specific amount of radiated energy. With Planck's law in mind, we know that this radiated energy is directly proportional to the radiated temperature, dependent on the viewed wavelengths. Other factors such as clouds and gas contamination can affect the observed radiated energy. Using Planck's constant and the following equation it is possible to find the temperature of the observed surface. An equation can be used to acquire temperature using known constants, wavelengths of light, emissivity and temperature:

(05) $T = (c_2)/\{\lambda \ln([\varepsilon c_1 \lambda^{-5}/\pi R_\lambda]+1)\}$

where c_1 is 3.742×10^{-16} W m^2 or $2\pi hc^2$, where c is the speed of light and h is Planck's constant, c_2 is 0.0144 m * K, K is hc/k (k is Boltzmann's constant) λ is wavelength or wavelength range of the viewed light in meters, R_λ is the radiance at the specific wavelength, ε is emissivity for the observed radiating surface, and finally, T is temperature in Kelvin (Matson and Dozier, 1981; Rothery et al., 1988).

Important Equations and Variables

There are other surface volcanic parameters that can be quantified from orbiting sensors using the Dual Band Equation (DBE), or equations adapted from the DBE. Within one pixel it is possible to calculate values for four important variables: T_c, T_h, f_h, and f_c. T_c is the temperature of the cooled portion of lava in the pixel. T_h is the temperature of the hot portion of lava in the pixel. f_h is area of hot lava within the pixel, while f_c is the area of cool lava within the pixel. By using one band of shortwave infrared data, and one band of thermal infrared data, and assuming for one of the following variables, T_c, T_h, and f_c, it is possible to solve for the other variables with the following equation adapted from the DBE;

$$(06) \quad L(T_X\lambda_X) = \varepsilon_X\tau_X \left[f_cL(T_c\lambda_X) + (1-f_c)L(T_h\lambda_X)\right]$$

The sub X value means one can express the entire equation for a specific band. L is the Planck function of a temperature T_X at the wavelength(s) λ_X for the band X. ε_X is the spectral emissivity for the viewed object and τ_X is the atmospheric transmissivity. Using equation 6 twice, with two different bands, allows the possibility to solve for T_c, T_h, and f_c if one of the variables is assumed. It is also possible to solve this equation using simultaneous equations with three different bands, but only know two of the variables. This allows the equations to be more accurate with fewer assumptions. If two bands are used in conjunction, only one assumption will be made. If three bands are used in conjunction the three variables can be used to solve for all three unknowns with no assumptions using the following equation adapted from the DBE;

$$(07) \quad R_X = \varepsilon_X\left[f_h(Rh_X) + (1-f_h)Rc_X\right]$$

where R_X is the pixel-integrated radiances for band x. Rh and Rc are the radiances associated with the two thermal variables, T_h and T_c (Lombardo et al., 2009).

These equations were used on volcanoes to examine sub-pixel variables. These sub-pixel variables, in this case f_h and T_c can be related to each other to classify different types of volcanic activity. As one moves down the slope of the volcano from the summit, it is possible to thermally distinguish the lava flows from proximal, medial-distal, and toe. The distribution of these variables will change depending on which thermal zone is viewed. Scatter plots of T_c vs f_h would show two distinct trends. The first trend would show that degassing activity plots as a near vertical trend parallel to the T_c axis, as seen in figure 4. The T_c values range from roughly 50 to 400 degrees Celsius with f_h values ranging from 0 to 0.002. The second trend is seen at lava flows with a logarithmic slope showing T_c increasing as f_h increasing, as seen in figure 2. This trend has been established as $y = 59\ Ln(x) + 667$ with T_c values ranging from 25 to 400 degrees Celsius, and f_h values from 0 to .007 (Lombardo et al., 2006).

After viewing the possible values for either degassing or lava flows activity, it is evident that distinguishing between the two types will be rather simple. This is extremely important to realize because it is possible to detect different volcanic activity solely from remotely sensed data and mathematical calculations.

Methods and Procedures

The Landsat TM sensor is the data source for this study. These data were chosen to coincide with the data used in the Lombardo et al. (2004) study. Working with a data source similar to the original study allows for more consistency and less error due to data differences, while allowing for similarities to be drawn with more accuracy. Landsat TM data have also been used in many studies over time to monitor volcanoes and have proven useful for the task (Harris et al. 1998, Lombardo et al., 2004; Flynn et al., 1994).

After the Landsat TM data for OL were obtained (shown in Table 5), the data were converted from 8-bit digital numbers to radiance in Watts per meters squared per micrometer per steradian. The Model Builder in ERDAS Imagine 2011 was used to perform the conversion. Equations 8, 9, and 10 were used to convert the Landsat TM data to radiance (Chander et al., 2009).

(08) L_λ = GRescale * Qcal + BRescale

(09)   GRescale = $LMAX_\lambda$ – $LMIN_\lambda$ / QCALMax – QCALMin

(10)   BRescale = $LMIN_\lambda$ – ($LMAX_\lambda$ – $LMIN_\lambda$ / QCALMax – QCALMin) * QCALMin

where Qcal is the input Landsat TM data in digital numbers, while L_λ is the output radiance in W/m2/μm/sr. The QCALMax and QCALMin values for the images used in the analysis are 255 and 1 respectively. This information is also found in the metadata for each Landsat TM file and can vary from image to image. $LMAX_\lambda$ and $LMIN_\lambda$ are the maximum and minimum radiance values, scaled to QCAL calibration coefficients in digital numbers, and are also found in the metadata file associated with each image. Over the lifetime of the Landsat TM sensor, the $LMAX_\lambda$ and $LMIN_\lambda$ values have been adjusted to accommodate for decay in the sensor for specific bands (Chander et al., 2009). As a result, the correct $LMAX_\lambda$ and $LMIN_\lambda$ values must be adapted for each image according to the Chander et al. (2009) numbers.

After the radiance file was created, a spatial subset of the image was created only containing OL for each image. This allowed for more efficient processing with less extraneous pixels, and also made visualization of images and results more straightforward as very low radiance values associated with vegetation or other non-volcanic features on the plains below the volcano are removed. With the above steps complete, the next step was to process the data using

the dual band equation to find values for T_c and f_h. These calculations were performed in ENVI + IDL using an IDL script. Certain variables must be set for the equations used to work properly, these include T_h, and T_b. The lava hot temperature, T_h is set to 817.15 Kelvin; this is equivalent to 544 degrees Celsius converted to Kelvin by adding 273.15. After much of the literature on OL was read, the hottest temperature from those lavas was observed at 544 Celsius (Krafft and Keller, 1989). Using 544 Celsius as the hottest temperature is important because we are assuming T_h to allow us to solve for T_c and f_h by using the Dual Band Equation. Most of the lavas at OL are very small in exposure and heat emanating from exposed lava is not likely to affect the surrounding pixels. With this reasoning, the background temperature T_b is set to 283.15 Kelvin equivalent to 10 degrees Celsius. Many values in the Band 6, the thermal band of Landsat 5 TM concur with these very low temperatures surrounding OL.

To help validate the procedure and calculations and accommodate the differences in sensors employed in the Lombardo study and the study describe here, data were also collected for Mt. Etna and processed according to their parameters. The procedures to convert the Landsat 5 TM data from digital numbers to radiance were identical for Mt. Etna and OL. To perform the Dual Band Equation for Mt. Etna some adjustment to variable values was necessary to adjust the script to function on data for a different location, with different volcanic characteristics (OL and Mt. Etna), so T_h was set to 1313.15 Kelvin and T_b was set to 398.15 Kelvin (Lombardo, 2012). Mt. Etna has a different composition than OL, and the DBE can be calculated properly by changing the variables T_h and T_b.

All the previous methods and procedures data was complied into Table 5. In Table 5, the usable pixels for analysis column represent the amount of pixels that successfully fit the

parameters of the dual band equation and this study. Every image was taken from Landsat 5 TM

except the 3/1/1989 image, which was taken from Landsat 4 TM.

Table 5. Landsat TM Image Dates Processed for the Analysis of OL and Mt. Etna

Oldoinyo Lengai	Mt. Etna	Satellite and Sensor	Usable pixels for analysis
	4/23/86	Landsat 5 TM	20
7/1/84		Landsat 5 TM	0
8/27/84		Landsat 5 TM	0
9/3/84		Landsat 5 TM	1
8/8/86		Landsat 5 TM	0
3/1/89		Landsat 4 TM	0
1/21/95		Landsat 5 TM	0
2/6/95		Landsat 5 TM	0
9/5/08		Landsat 5 TM	0
9/21/08		Landsat 5 TM	0
6/4/09		Landsat 5 TM	0
7/6/09		Landsat 5 TM	0
11/27/09		Landsat 5 TM	0
1/30/10		Landsat 5 TM	0
7/9/10		Landsat 5 TM	0
1/17/11		Landsat 5 TM	0
7/12/11		Landsat 5 TM	0

To further validate that the parameters for OL calculated with valid results, the same

calculations used for OL were performed using the 4/23/1986 image of Mt. Etna. In this case,

the theoretical background temperature (T_b) and theoretical hot lava temperature (T_h)

parameters would be set lower than the true observed values to assist in proving the script runs

properly, as described above. The calculations performed have the possibility to generate

unrealistic values with either negative area (f_h values) or negative temperature (T_c values). If

the calculations run properly, it would prove that the script produces realistic data. The data

produced would not necessarily be valid because of using incorrect values for T_b and T_h, but would prove that the theoretical calculations running for the OL images are run correctly.

To test the sensitivity of the model, the September 3, 1984 image was processed with a range of hot temperatures (T_h). This was done to see at what temperatures the model would be more accurate and produce more data. The image was processed with temperatures in an increment of 100 degrees Celsius from 100 to 1100 degrees Celsius.

CHAPTER 5

RESULTS

Results for Oldoinyo Lengai

In this study, the main objective was to detect and verify lava flow and degassing activity at Oldoinyo Lengai. This is an objective because this type of volcanic activity detection has been successfully conducted at Mt. Etna but not at volcanoes with irregular compositions such as Oldoinyo Lengai. The overarching idea is if this analysis works correctly, we can continue to apply these methods to other volcanoes with irregular compositions around the world. To do this, the analysis was performed and the results were then concluded.

The procedures listed in previous chapters were performed on sixteen images of OL over a range of dates from 1984 to 2011 and ran properly for all the images. This type of analysis yields a number of pixels, which are capable of producing sub-pixel variables of interest for characterizing volcanic activity. Ideally, a large number of valid pixels need to be produced for proper analysis because these pixels need to be graphed, and once they are graphed, trends can be established to determine if the data represents either lava flow or degassing activity based from the Lombardo et al. (2006) study. A pixel is considered valid when it fulfills all the requirements for the dual band equation, while being calculated with the correct variables for the specific lava composition associated with the volcano being observed. There was only one image that yielded one valid pixel. The image from September 3, 1984 yielded one valid pixel

with a maximum temperature (T_c) of 12.6554 Celsius with a fractional area (f_h) of 0.0100224.

The temperature for this pixel is not likely to represent a lava flow or degassing activity, because

the temperature value (T_c) is too low. This pixel is likely to represent higher than background

temperature, which is essentially insignificant due to its very low temperature. This pixel can be

seen in Figure 7. This shows the distribution of values of f_h vs T_c. The distribution of pixels for

the Mt. Etna data implies this is a group of degassing pixels because the values do not exceed

.002 f_h and are below 400 degrees Celsius, which is consistent with the trend for degassing

activity as stated before. Figure 7 also contains the single valid pixel solved from the Oldoinyo

Lengai analyses, in this case from 9/3/1984.

The other images processed at OL did not resolve any other valid pixel data, indicated by

the dual band equation failing to resolve any data from the images processed. At OL more valid

pixels would need to be properly calculated to further establish any data trends, which would

then be used to distinguish lava flow or degassing activity. In other words, the analysis did not

yield results which would allow for differentiating volcanic activity of various types.

Given a concern that the methods of analysis were incorrect, the same analysis was

repeated for one image covering Mt. Etna from April 23rd, 1986. A full list of the 20 valid pixel

values can be seen in Table 7. The fractional areas of valid pixels ranged from 1.660×10^{-5} to

1.002×10^{-3}, with temperatures ranging from 134.5 to 258.0 degrees Celsius. These values

produced fall within the acceptable range of values for Landsat TM data. The values fall within

and slightly beyond the typical range of values described by Lombardo et al. (2004), with their

values of f_h ranging from 0 to 0.001, and T_c values occurring below the theoretical oblique line

of $T_c = 258,823 * f_h - 40$. This analysis verified that the analysis methods were indeed correct,

yielding valid results within known ranges for a different volcano with accurate theoretical variable values representing conditions of that volcano.

Given that the analysis methods appeared sound according to the results for the Mt. Etna image and applicable variables, a further concern could be that the parameters for OL, though indicated through field studies (Krafft and Keller, 1989), may be invalid, preventing results from being calculated. To address this, the final procedure was to perform the analysis on the Mt. Etna image using the theoretical parameters for OL to verify they are capable of producing results given pixels containing areas of volcanic activity. The analysis was performed on the Mt. Etna image by setting T_h (the hottest temperature possible for lava flows at OL) to 544 Celsius, and T_b (the ambient background temperature) to 10 degrees Celsius. T_h is a theoretical parameter that is used to limit the output data to realistic results. Negative temperatures and negative areas are limited from the results to keep only realistic values in the output. The calculations for Mt. Etna, using the T_h and T_b values for OL were used for the analysis to help verify the procedures. These ran and produced 7 pixels and can be seen in Table 6.

Table 6. All Pixels Produced by the Analysis for the March 23, 1986 Landsat TM Image of Mt. Etna

Pixel Number	Fractional Area	Temperature in Celsius
1	0.0100205	12.6535740
2	0.0100202	12.6563263
3	0.0100321	12.6496458
4	0.0115157	166.9952087
5	0.0036023	249.5779724
6	0.0056172	175.9721222
7	0.0009320	73.5562668

Pixels 4 through 7 represent lava flows, but pixels 1 through 3 do not appear to represent significant temperatures from thermal activity. Because the calculations generated an output with realistic fractional area and temperatures, this shows the analysis of Mt. Etna using the theoretical parameters for OL can generate values of f_h and T_c, despite deliberately using incorrect theoretical parameters (the hottest temperature, and background temperature were set lower than would normally for the composition at Mt. Etna). The pixels that were generated are used to simply test the validity of the analysis, not necessarily to produce usable results. This bolsters the analysis and procedure by proving that script runs and can produce results with realistic values. All the following results and procedures are summarized in the flowchart of Figure 6 with the programs and data conversions used described in each step.

Figure 6. A Flowchart Showing a List of the Procedures Used for the Analysis

Step 1: Obtained input Oldoinyo Lengai Landsat TM data.

Step 2: Converted 8-bit Landsat data to radiance, using Model Builder.

Step 3: Created spatial subset image to constrain analysis to study area.

Step 4: Determined correct values for variables T_h and T_b, based on volcanic composition.

Step 5: Preformed dual band calculation on data to find T_c and f_h, using ENVI + IDL.

Step 6: Ploted T_c and f_h using scatterplot graph, in Microsoft Excel.

Step 7: Determined if a relationship existed between T_c and f_h.

Step 8: Obtained input Landsat TM data for Mt. Etna.

Step 9: Repeated steps 1 through 7 for Mt. Etna data.

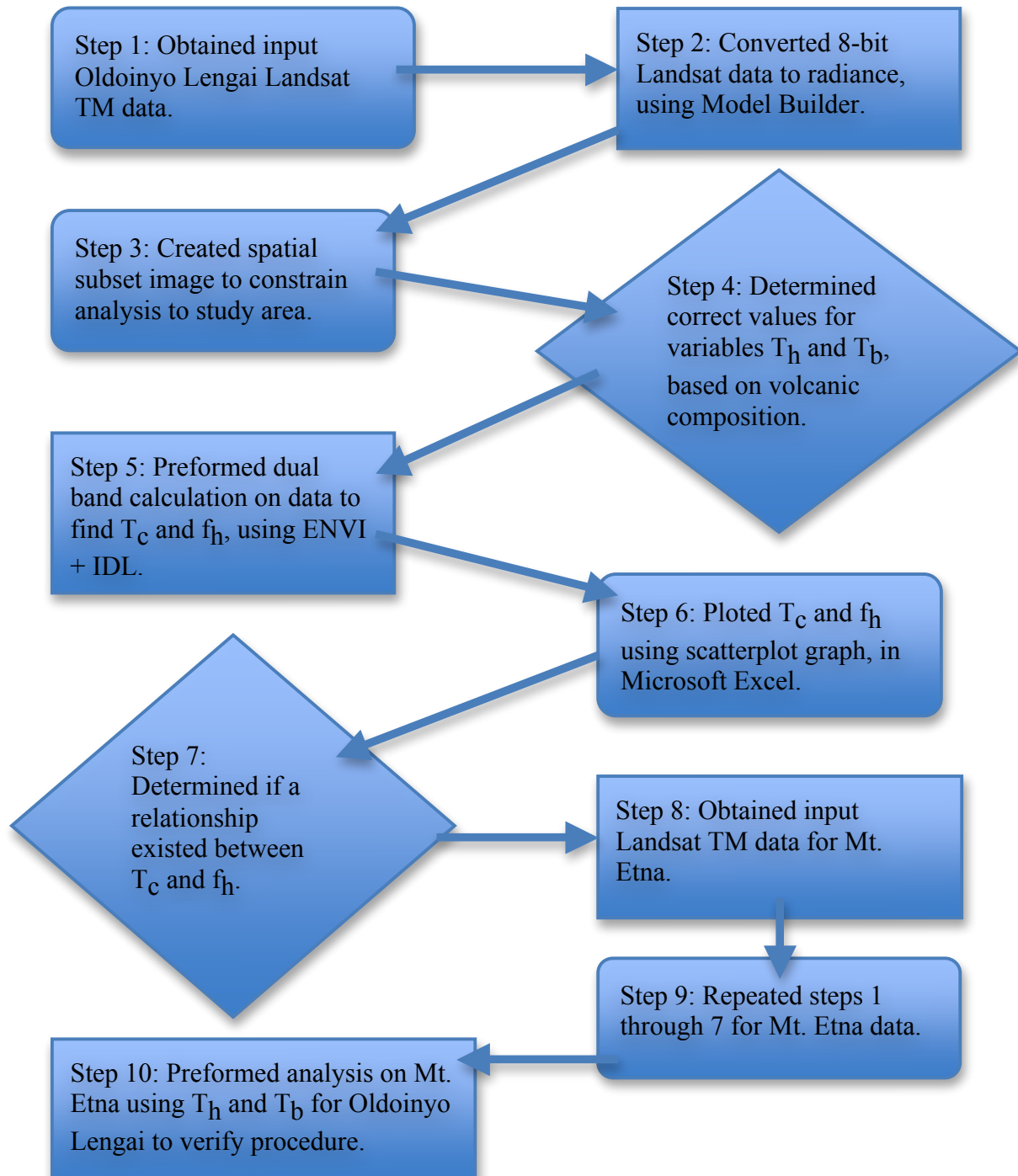Step 10: Preformed analysis on Mt. Etna using T_h and T_b for Oldoinyo Lengai to verify procedure.

Table 7. Pixels Calculated from the April 23, 1986 Image of Mt. Etna

Pixel Number	Fractional Area	Temperature in Celsius
1	0.0006618	134.5395050
2	0.0008177	158.1901703
3	0.0006668	182.9865875
4	0.0005421	231.6440125
5	0.0001398	191.1109924
6	0.0004588	137.6051788
7	0.0003932	162.4955597
8	0.0002941	218.9640198
9	0.0006433	219.9897003
10	0.0006615	231.6518250
11	0.0010020	148.9614563
12	0.0003292	240.6936035
13	0.0001834	239.0741730
14	0.0000527	257.9993591
15	0.0000914	218.6055908
16	0.0000964	178.6741028
17	0.0001855	192.1280060
18	0.0002095	149.5009155
19	0.0001448	155.8162689
20	0.0000166	149.7733612

Figure 7. Results for Mt. Etna on 04/23/1986 and Oldoinyo Lengai on 9/3/1984
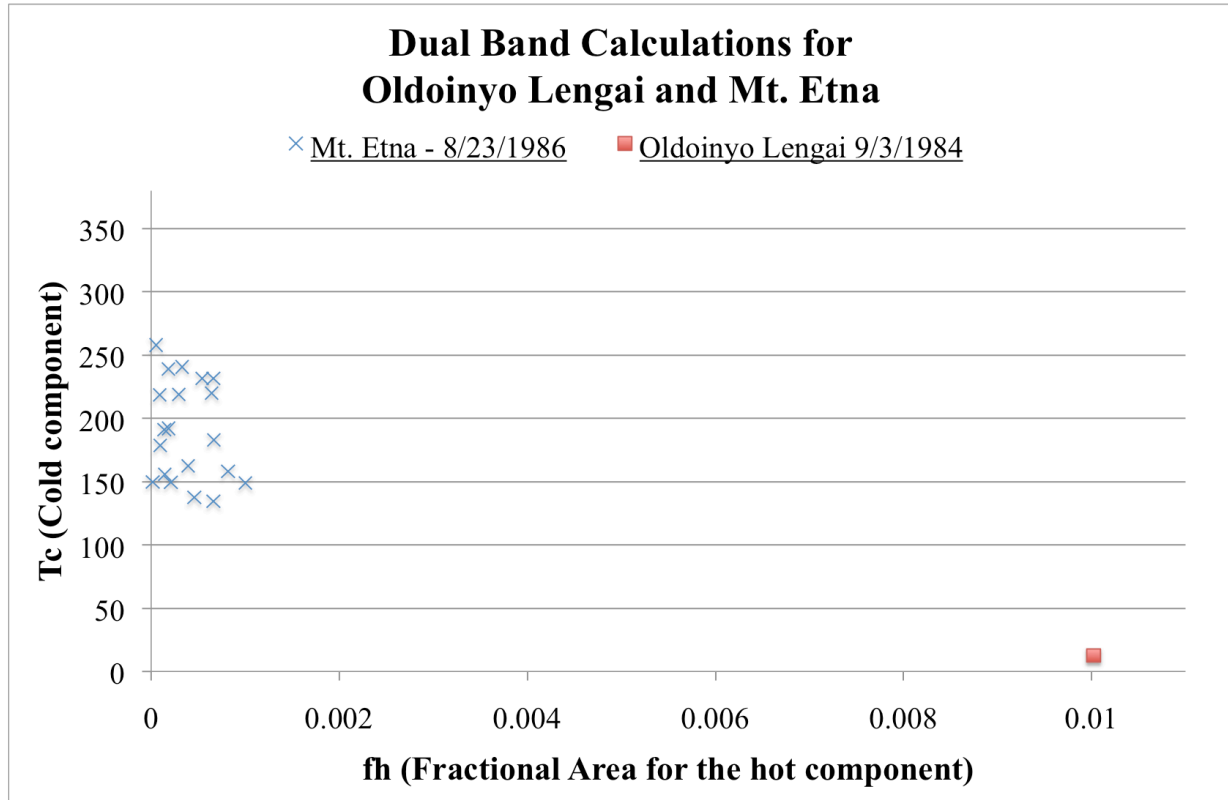
The sensitivity analysis was conducted to see at what theoretical hot lava temperatures (T_h) would be more sensitive. This would show at what temperatures the Landsat TM sensor would respond with more accuracy. The resulting output pixel analysis can be seen in Table 8, showing a T_h ranging from 100 to 1100 Celsius.

Table 8. Sensitivity Analysis Showing Results of September 3, 1984 Analysis for Oldoinyo

Lengai

Theoretical Hot Temperature in Celsius	Resulting Temperature in Celsius	Fractional Area
100	no results	no results
200	no results	no results
300	no results	no results
400	no results	no results
500	no results	no results
544	12.6554213	0.0100224
600	12.6499000	0.0100113
700	no results	no results
800	198.7725067	0.0026646
900	138.5361633	0.0018276
	223.7655182	0.0013186
	117.5925827	0.0018486
1000	200.9768219	0.0010173
	235.5239410	0.0007287
	196.1954803	0.0010418
	198.6547852	0.0010296
1100	219.1319275	0.0006154
	242.5656128	0.0004393
	173.1763611	0.0004745
	216.4294434	0.0006304
	217.8007660	0.0006229

CHAPTER 6

DISCUSSION, FURTHER RESEARCH, AND CONCLUSIONS

Discussion

After processing 16 Landsat TM images, only one pixel was produced at OL which could be used to calculate f_h and T_c. This pixel was produced for the September 3rd 1984 image with a temperature of 12.6554 degrees Celsius and a fractional area of 0.0100224. Because the resulting pixel produced from the analysis is not sufficient to plot relationships between important characteristics allowing for the separation of volcanic activity types, more pixels would be needed to be generated complete results. If such a trend were to be observed, it would be possible to distinguish either lava flow or degassing activity. Unfortunately, that was not the case for OL over the years 1984 to 2011, where it was attempted (see Table 5).

To validate that the analysis procedure was valid, an image of Mt. Etna was processed. Those calculations produced 20 valid pixels within a reasonable range of values, similar to those described by Lombardo et al. (2004) using Landsat TM. By running the analysis on an image of Mt. Etna, it is clear that the script generates valid results, which are compatible with those calculated with a different sensor, thereby removing any question that results may not be valid due to sensor differences. In other words, since the only difference between the script as parameterized for Mt. Etna and as parameterized for OL are the theoretical variables T_b and T_h, this proves that the fashion in which the calculations were made is valid. A sensitivity analysis

was also conducted to see how responsive the analysis is to different theoretical hot lava

temperatures. This was conducted by changing the T_h with values of 100 to 1100 degrees

Celsius. The analysis shows no response for lower temperatures until the valid T_h 544 degrees

Celsius. The amount of resulting data is sporadic until 900 degrees Celsius. The amount of

resulting data consistently increases with 3 pixels at 900 degrees, 4 pixels at 1000 degrees, and 5

pixels at 1100 degrees Celsius. This implies that the calculations are more responsive to lavas

with higher temperatures preferably over 900 degrees Celsius.

To further validate the calculations for the script used on the OL images, the Mt. Etna

image was used as an input with the variables T_b and T_h for OL instead of those for Mt. Etna.

This allows for the evaluation that the theoretical variables T_b and T_h used for OL can also

produce results. Indeed, the resulting output shows 11 pixels with volcanic activity. Running the

script in this way, and achieving results addressed the concern that the script may generate

negative areas and numbers for the variables f_h and T_c, which would constitute invalid results.

The output values of T_c and f_h are constrained to realistic values by using theoretical variables

T_h and T_b for the lava and sensor characteristics. By determining that the code runs correctly,

returning valid results, the lack of pixels produced from the analysis could not be due to either

analysis procedures or calculation error.

In this study of OL there are numerous problems that could be addressed. The biggest

and most significant problem is the availability of Landsat scenes covering OL during periods

where lavas are exposed. Many of the lava flows occurring at OL are confined to the hornitos

within the summit crater, which occur over a range of small areas but more significantly smaller

than the 30 meter pixel size of Landsat TM data. In the volcanic history of OL, there are only a

few cases where lava flows occur with large spatial extent, and those instances only occur when

lava spills over the crater walls (Dawson et al., 1994). In these cases, Landsat scenes were unavailable for those periods. Smaller lava flows make detection particularly difficult for this analysis due to the relatively coarse spatial resolution from the Landsat TM sensor. The study would have benefitted from thermal anomalies with greater spatial extent.

Along with the chance to capture thermal information for much larger anomalies through more cloud-free imagery, the analysis would benefit from higher spatial and spectral resolution data. Each pixel for which key variables were calculated has a specific area. The smaller the area each pixel covers, the more pixels can be included in the analysis. By using a sensor with higher spatial resolution, more pixels could be detected more accurately, resulting in more observations for the same size thermal anomaly. In addition, as saturation of pixels was also an issue with the analysis, greater spectral resolution would be ideal. Pixel saturation occurs if the light measured by a specific band becomes intense enough to produce a maximum response, in this case a digital number value of 255. Landsat TM bands 5 and 7 have wavelengths through a large range of light, essentially lowering the maximum response of the sensor, resulting in a greater chance for spectral saturation of pixels. Many of the newer hyperspectral satellites and airborne sensors have bandwidths which are much narrower, allowing for higher responses and preventing pixel saturation from occurring, or at least from occurring as often. Indeed, this is one reason why Lombardo et al. (2006) used the DAIS sensor in their study of Mt. Etna. While using hyperspectral data would benefit the analysis, in this study one goal was to use easily accessible and economical (in this case free) data to see if such data could be used in global volcanic monitoring.

Further Research

This study shows that more avenues need to be pursued in relation to remote sensing

applications for volcanic monitoring. Nighttime data in some cases are available for these

volcanoes. The nighttime imaging would benefit the analysis by lowering the background

temperature allowing for the thermal response to contain less erroneous thermal data. It would

also be prudent to look at major factors altering the trend between f_h and T_c, such as pixel size

and how that can affect the relationship could yield intriguing results, and also indicate the

minimum spatial resolution at which relationships can be calculated for volcanoes of various

sizes. Furthermore, the relationship between f_h and T_c could change for different composition

volcanoes and for various resolutions of data. One approach to test this would be to resample

fine-resolution data to coarser spatial resolutions. This might prove useful when attempting to

analyze similar volcanoes with different resolution input data.

Performing the analysis on other volcanoes with a different composition could also be

analyzed, such as the andesitic volcano Shiveluch in Russia because it has produced larger lava

flows than OL (GVP, 2012), and would allow for the correlation of lava flow and degassing

trends across different volcanic compositions. Correlating these trends may allow for the

establishment of a relationship from one volcanic composition to another.

In many cases, volcanoes are automatically scanned for thermal anomalies to indicate

activity. If remote sensing methods for detecting lava flows and gaseous activity become

reliably established, then adding this detection into global volcanic monitoring automation,

would allow for more precise assessments on the current activity of a volcano. As newer sensors

are developed with higher spatial, spectral, and temporal (allowing for greater data coverage)

resolution, obtaining more accurate results with the analysis technique explored in this document

might become commonplace. If superior sensors such as hyperspectral, ASTER, or Landsat Data Continuity Mission were used, then the higher spatial, spectral, and radiometric resolution would benefit the analysis by increasing the amount of usable pixels, reduce the amount of saturated pixels, and increase the pixel depth. HyspIRI is another hyperspectral sensor in production that is designed with volcanic remote sensing as a main application. It contains contiguous 10 nanometer bands from 380 to 2500 nanometers (JPL, 2012). This makes it possible to gain more knowledge about the volcano, and would increase the overall effectiveness of volcanic remote sensing.

Conclusions

In continuing to improve techniques, analysis and effectiveness should always be at the forefront of scientific research, including volcanic remote sensing. The study proved that the calculations ran properly, but the input data was insufficient to perform the analysis with usable results. Higher spatial, spectral, radiometric and temporal resolution are needed for a more complete analysis. This study would have benefited from a larger volcano with larger lava flows. This study shows the potential for this analysis to produce helpful results in turn determining more information about volcanoes and their activity at an earlier stage. Further research can produce extremely valuable insight that will further the study of volcanic remote sensing in the future.

REFERENCES

Chander, G., Markham, B., & Helder, D. (2009). Summary of current radiometric calibration coefficients for Landsat MSS, TM, ETM+, and EO-1 ALI sensors. *Remote Sensing of Environment, 113*, 893-903.

Corsaro, R. A., & Pompilio, M. (2004). Magma dynamics in the shallow plumbing system of Mt. Etna as recorded by compositional variations in volcanics of recent summit activity (1995-1999). *Journal of Volcanology and Geothermal Research, 137*, 55-71.

Dawson, J. B. (1962). The geology of Oldoinyo Lengai. *Bulletin volcanologique; organe de la Section de volcanologie de l'Union ge'ode'sique et ge'ophysique internationale, 24*, 348-387.

Dawson, J. B., Pinkerton, H., Norton, G. E., & Pyle, D. M. (1990). Physiochemical properties of alkai carbonatite lavas, Data from the 1988 eruption of Oldoinyo Lengai, Tanzania. *Geology, 18*, 260-263.

Dawson, J. B., Pinkerton, H., Pyle, D. M., & Nyamweru, C. (1994). June 1993 eruption of Oldoinyo Lengai, Tanzania Exceptionally viscous and large carbonatite lava flows and evidence for coexisting silicate and carbonate magmas. *Geology, 22*, 799-802.

Dozier, J. (1981). A Method for Satellite Identification of Surface Temperature Fields of Subpixel Resolution. *Remote Sensing of Environment, 11*, 221-229.

DuBois, Furst, J., Guest, N., & Jennings, D. (1963). Fresh Natro Carbonatite Lava from Oldoinyo L'Engai. *Nature, 197*, 445-446.

Flynn, L. P., Harris, A. J. L., & Wright, R. (2001). Improved identification of volcanic features using Landsat 7 ETM+. *Remote Sensing of the Environment, 78*, 180-193.

Flynn, L. P., Harris, A. J. L., & Wright, R. (2001). Improved identification of volcanic features using Landsat 7 ETM+. *Remote Sensing of the Environment, 78*, 180-193.

GVP. (2011a). Etna. Retrieved Saturday April 30th, 2011, from

http://www.volcano.si.edu/world/volcano.cfm?vnum=0101-06=

GVP. (2011b). Ol Doinyo Lengai. Retrieved Saturday April 30th, 2011, from

http://www.volcano.si.edu/world/volcano.cfm?vnum=0202-12=

GVP. (2012). Shiveluch. Retrieved Monday August 27th, 2012, from

http://www.volcano.si.edu/world/volcano.cfm?vnum=1000-27=

JPL. (2012). HyspIRI Mission Study Website. Retrieved Nov 6 2012, 2012, from

http://hyspiri.jpl.nasa.gov/

Harris, Flynn, Keszthelyi, Mouginis-Mark, Rowland, & Resing. (1998). Calculation of lava effusion rates from Landsat TM data. *Bulletin of Volcanology, 60*, 52-71.

Keller, J., Klaudius, J., Kervyn, M., Ernst, G., & Mattsson, H. (2010). Fundamental changes in the activity of the natrocarbonatitie volcano Oldoinyo Lengai, Tanzania. *Bulletin of Volcanology, 72*, 893-912.

Krafft, M., & Keller, J. (1989). Temperature Measurements in Carbonatite Lava Lakes and Flows from Oldoinyo Lengai, Tanzania. *Science, 245*(4914), 168-170.

Lombardo, V. (2012). Dual-band Calculation Program performed for ASTER sensor images in Interactive Data Language Executable Code, Provided by the Author via Personal Communication.

Lombardo, V., Buongiorno, M., Pieri, D., & Merucci, L. (2004). Differences in Landsat TM derived lava flow thermal structures during summit and flank eruption at Mount Etna. *Journal of Volcanology and Geothermal Research, 134*, 15-34.

Lombardo, V., Buongiorno, M. F., & Amici, S. (2006). Characterization of volcanic thermal anomalies by means of sub-pixel temperature distribution analysis. *Bulletin of Volcanology, 68*, 641-651.

Lombardo, V., Harris, A. J. L., Calvari, S., & Muongiorno, M. F. (2009). Spatial Variations in lava flow field thermal structure and effusion rate derived from very high spatial hyperspectral (MIVIS) data. *Journal of Geophysical Research, 114*(B02208).

Matson, M., & Dozier, J. (1981). Identification of Subresolution High Temperature Sources Using a Thermal IR Sensor. *Photogrammetric Engineering and Remote Sensing, 47*(9), 1311-1318.

Rothery, D. A., Francis, P. W., & Wood, C. A. (1988). Volcano Monitoring Using Short Wavelength Data from Satellites. *Journal of Geophysical Research, 93*(B7), 7993-8008.

Vaughan, R. G., Kervyn, M., Realmuto, V., Abrams, M., & Hook, S. J. (2008). Satellite measurements of recent volcanic activity at Oldoinyo Lengai, Tanzania. *Journal of Volcanology and Geothermal Research, 173*, 196-206.

Zaitsev, A., & Keller, J. (2006). Mineralogical and chemical transformation of Oldoinyo Lengai natrocarbonatites, Tanzania. *Lithos, 91*, 191-207.